Supplemental Material for
Bragg diffraction of large organic molecules

Christian Brand,[1,2] Filip Kiałka,[1,3] Stephan Troyer,[1] Christian Knobloch,[1] Ksenija
Simonović,[1] Benjamin A. Stickler,[3,4] Klaus Hornberger,[3] and Markus Arndt[1,*]

[1]*University of Vienna, Faculty of Physics, Boltzmanngasse 5, A-1090 Vienna, Austria*
[2]*German Aerospace Center (DLR), Institute of Quantum Technologies, Söflinger Straße 100, 89077 Ulm, Germany*
[3]*Faculty of Physics, University of Duisburg-Essen, Lotharstraße 1, 47048 Duisburg, Germany*
[4]*QOLS, Blackett Laboratory, Imperial College London, SW7 2AZ London, United Kingdom*
(Dated: June 17, 2020)

LASER DESORPTION

We employ a tightly focused laser beam to thermally evaporate the molecules. This results in a high thermal load which may lead to thermal decomposition of ciprofloxacin, especially the detachment of the carboxyl group (-COOH). As the experimental setup offers no mass resolution, this might deteriorate the contrast of the observed pattern. To test whether fragmentation occurs in our source, we desorbed ciprofloxacin in high vacuum and collected the material 8 mm behind the source. This sample was analyzed using matrix-assisted laser desorption/ionization mass spectrometry and compared to the pristine sample from the supplier. The mass spectra show that the laser evaporation leaves more than 99% of ciprofloxacin intact. For phthalocyanine this has been tested with the same result [22].

FLUORESCENCE IMAGING

To visualize the diffraction images of ciprofloxacin, we illuminate the pattern with about 100 mW of 266 nm light generated by a SIRAH WAVETRAIN 2 pumped by a CO-HERENT VERDI V10. We use a rotating diffuser to achieve uniform illumination at a grazing angle of incidence. The fluorescence photons are collected via a 20-fold microscope objective (ZEISS PLANNEO FLUAR, NA = 0.5) and separated from the background via a bandpass filter transmitting light in the range between 505 and 595 nm. The images are recorded with a UV enhanced EMCCD camera (ANDOR iXON DV885 - K(S-VP)), using a multiplication factor of 1 and an integration time of 20 s. Background-correction was achieved by subtracting images under identical illumination with and without molecules.

The patterns of phthalocyanine are recorded by illuminating the pattern with 661 nm light and recording the fluorescence in the range between 700 and 725 nm. For more details see Refs. [23, 24].

DATA PROCESSING — CIPROFLOXACIN

We perform data processing of all diffraction images using the SCIPY stack. For Fig. 2a) we averaged 6 individual images of the deposited pattern and denoised the result with
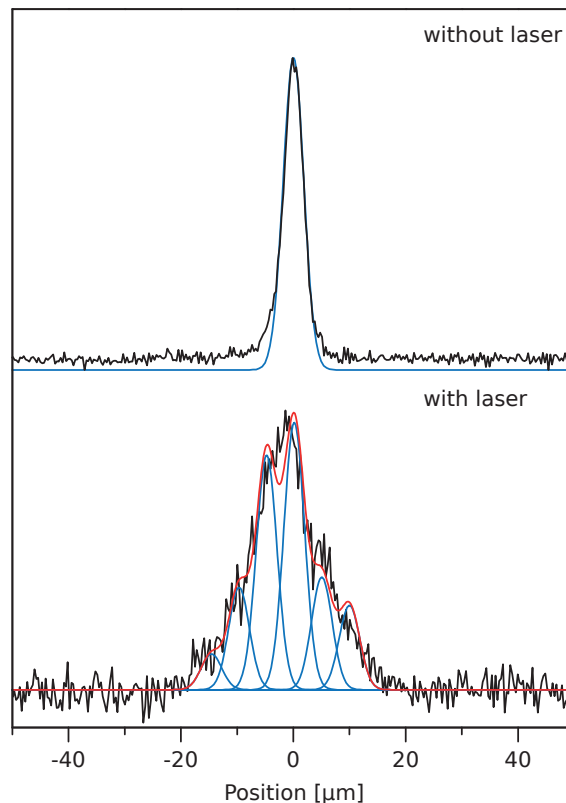
Suppl. Fig. 1. a) Collimating a beam of phthalocyanine with the S_x delimiter set to 4 μm leads to a Gaussian signal with a $1/e^2$ radius of $w_x = 4.4(1)$ μm at the detector. b) Inside a 30 W laser beam the molecules absorb a mean number of 2 to 3 photons for $v = 140$ m/s resulting in a broadened pattern. The spacing of the peaks (4.9 μm) matches the recoil of a single 532 nm photon and the resolved substructure suggests that re-emission after absorption is not the dominant deexcitation mechanism.

a Gaussian filter with a radius of 1 camera pixel. We then perform background correction (in addition to the background subtraction done after image acquisition) by masking the diffraction pattern, averaging the image along the y-direction, fitting a smoothing spline, and subtracting the noise floor. The same process is repeated along the x-axis. To find the horizontal center of the diffraction pattern we fit a Gaussian to a y-averaged, 16 μm wide horizontal stripe at the top of the diffraction pattern.
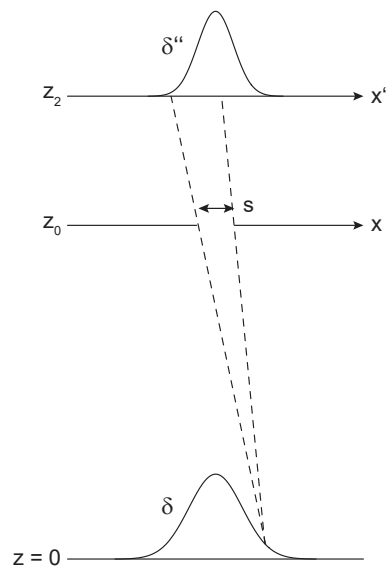
DATA PROCESSING — PHTHALOCYANINE

We determine the forward velocities in the images by comparison with a phthalocyanine diffraction pattern obtained with a material grating in Ref. [24]. The patterns are aligned by maximizing the overlap of their intensity distributions, which are obtained by integrating the images horizontally. For a material grating the diffraction orders are clearly separated, and the position- as well as momentum-space separation between them is known, which allows us to calculate the forward velocities.

To align the profiles in Fig. 4d) we fit them with a sum of three Gaussians, two narrow ones for the peaks and a broad one to account for the losses. The profiles and images are then horizontally aligned with respect to the rightmost Gaussian for negative incidence angles and the leftmost Gaussian for positive incidence angles. By taking into account the molecules' forward velocity, we convert the horizontal axis from pixel to $\hbar k$.


Suppl. Fig. 2. Estimating the effective source size δ and the collimation radius of the molecular beam from the known on-screen stripe radius δ'' and collimation slit width s. The Gaussian peaks represent the (approximately Gaussian) molecular densities in the source and detector planes.

NUMERICAL SIMULATION — CIPROFLOXACIN

The diffraction image shown in Fig. 2b) is simulated line-by-line (horizontally) by solving the Raman-Nath equations (4) using QuTiP [25, 26]. We truncate the infinite set of equations to those with $|j| < 2^{13}$ and choose $n = 700$. The initial state is Gaussian in position space with a parabolic phase and a standard deviation of the probability amplitude equal to 4.6 μm. The latter is chosen so that the width of the undiffracted beam at the top of the experimental image matches that in the simulation with the laser turned off. The parabolic phase, in turn, is that of a paraxially-approximated spherical wave with the source located 1505 mm (the distance between the source and the S_x delimiter) away. We start by transforming the initial state to momentum space via FFT and evolving it using QuTiP's `sesolve` with a time-dependent, band-diagonal Hamiltonian. We integrate the Schrödinger equation over a time interval of $6\sigma\omega_r^{-1}$, after which free propagation in momentum space (by multiplication with the transfer function in Fresnel approximation) is performed. The result is then transformed back to position space. The resulting lines of the simulation are stacked vertically and multiplied by the intensity of the corresponding data line. Then, a Gaussian filter is applied in the vertical direction to the obtained image to account for the finite height of S_y. To account for the horizontal extent of the source (and thus finite transverse coherence), we calculate 50 diffraction patterns for point sources with different x positions and average the images by intensity with Gaussian weights corresponding to an estimated source radius of 12 μm standard deviation.

ABSORPTION INSIDE THE GRATING

To estimate the number of photons phthalocyanine absorbs inside the laser grating, we limit the transverse velocity spread in the molecular beam to about the recoil velocity by closing the S_x delimiter to 4 μm. For molecules traveling at 140 m/s, this leads to a most probable transverse velocity of 0.4 mm/s, which corresponds to a kinetic energy of about 5 nK in this degree of freedom. With the laser grating turned off, the signal at the detector has a $1/e^2$ radius of $4.4(1)$ μm as shown in Suppl. Fig. 1a). Turning on the grating with a power of 30 W, vertical radius $w_y = 44(1)$ μm, and incidence angle $\theta_{\text{grat}} = 1.25$ mrad, for which we expect no diffraction, results in a broadening of the beam as shown in Suppl. Fig. 1b). The lineshape exhibits a substructure whose spacing matches the recoil of a 532 nm photon for molecules travelling at 140 m/s, assuming that the width of the individual peaks remains constant. From the shape we infer that the mean number of absorbed photons is about 2.5 at this laser intensity, and thus in the range 0.8–1.0 at the intensities used in the diffraction experiments.

MOLECULAR BEAM COLLIMATION

To estimate the collimation radius of the molecular beam, we first estimate the source size using ray optics, as illustrated in Suppl. Fig. 2. For an infinitely narrow collimation slit at $z = z_0$ and Gaussian source (at $z = 0$) with standard deviation δ, we would expect a Gaussian stripe on screen with
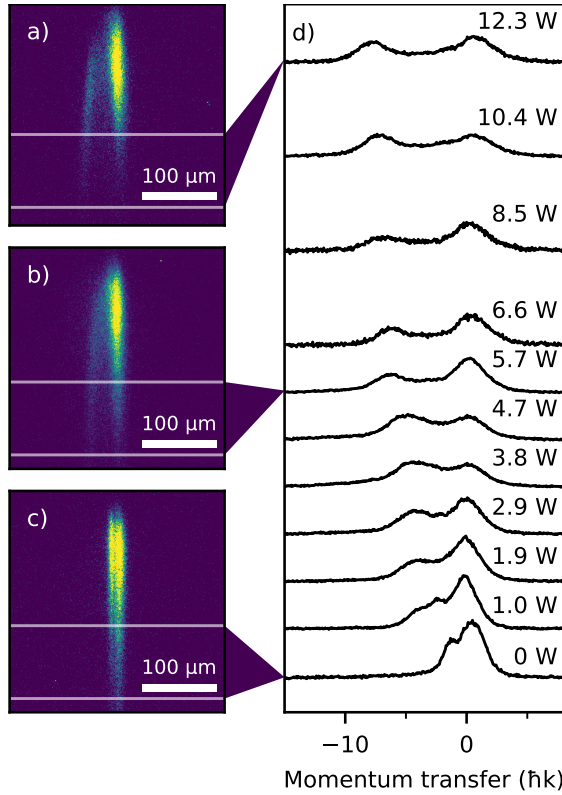
Suppl. Fig. 3. Power dependence of Bragg diffraction of phthalocyanine. Panels (a) and (b) show the diffraction patterns for laser grating powers of 12.3 (a) and 5.7 W (b). The double peak visible at 0 W (c) is an artifact caused by the collimation slit. Panel (d) shows intensity profiles integrated over a region corresponding to a velocity range of 143–175 m/s.

width

$$\delta' = \frac{z_2 - z_0}{z_0}\delta. \tag{SI.1}$$

If the slit has finite width described by a transmission function $t(x)$, the stripe on screen will be a convolution of the δ'-wide Gaussian with a projection of the slit, $t\left((z_0/z_2)x'\right)$. To obtain a simple analytical estimate of the stripe width, we approximate a boxcar-shaped $t(x)$ with a Gaussian with a standard deviation of $s/4$. The stripe is then also Gaussian with a standard deviation

$$\delta'' = \sqrt{\left(\frac{sz_2}{4z_0}\right)^2 + \left(\frac{z_2 - z_0}{z_0}\delta\right)^2}. \tag{SI.2}$$

Eq. (SI.2) is easily inverted, allowing us to estimate δ knowing s and δ''. With a known source size δ and slit size s we can estimate the one-sigma collimation radius to be

$$\frac{1}{z_0}\left(\delta + \frac{s}{2}\right). \tag{SI.3}$$

Using Eq. (SI.2) we estimate the source sizes to be 12 and 10 µm for the data in Figs. 3 and 4, respectively. This gives one-sigma collimation radii of 12 µrad in both cases (the two-sigma collimation radii are 20 and 19 µrad, respectively).

EFFECT OF GRATING POWER

To study the influence of the potential depth on the diffraction efficiency, we record diffraction patterns at grating powers ranging from 0 up to 12.3 W, as shown in Suppl. Fig. 3. The profiles in panel (d) show the intensity oscillating between the diffracted and the undiffracted beams. Additionally, the distance between the peaks increases as a function of power, corresponding to a change in θ_{grat} of about 20 µrad. We attribute this to residual thermal drift in the experimental setup.

---

[*] markus.arndt@univie.ac.at
[22] C. Knobloch, *Coherent matter-wave manipulation techniques*, Ph.D. thesis (2019).
[23] T. Juffmann, A. Milic, M. Müllneritsch, P. Asenbaum, A. Tsukernik, J. Tüxen, M. Mayor, O. Cheshnovsky, and M. Arndt, Nat. Nanotechnol. **7**, 297 (2012).
[24] J. P. Cotter, C. Brand, C. Knobloch, Y. Lilach, O. Cheshnovsky, and M. Arndt, Sci. Adv. **3**, e1607478 (2017).
[25] J. Johansson, P. Nation, and F. Nori, Comput. Phys. Commun. **183**, 1760 (2012).
[26] J. Johansson, P. Nation, and F. Nori, Comput. Phys. Commun. **184**, 1234 (2013).